Physics of Fluids

Time resolved measurements of droplet preferential concentration in homogeneous isotropic turbulence without mean flow

Cite as: Phys. Fluids **31**, 025103 (2019); https://doi.org/10.1063/1.5063673
Submitted: 29 September 2018 . Accepted: 14 January 2019 . Published Online: 04 February 2019

H. Lian, X. Y. Chang, and Y. Hardalupas

Physics of Fluids ARTICLE scitation.org/journal/phf

Time resolved measurements of droplet preferential concentration in homogeneous isotropic turbulence without mean flow

Cite as: Phys. Fluids 31, 025103 (2019); doi: 10.1063/1.5063673
Submitted: 29 September 2018 • Accepted: 14 January 2019 •
Published Online: 4 February 2019

H. Lian,[1] X. Y. Chang,[1] and Y. Hardalupas[2,a)]

AFFILIATIONS

[1]Institute of Mechanics, Chinese Academy of Sciences, 100190 Beijing, People's Republic of China
[2]Department of Mechanical Engineering, Imperial College London, SW7 2AZ London, United Kingdom

[a)]Author to whom correspondence should be addressed: y.hardalupas@imperial.ac.uk

ABSTRACT

An experimental investigation of the time-dependent spatial distribution of droplet concentration in a "box" of stationary homogeneous and isotropic turbulence without mean flow was performed for polydispersed droplet clouds with a wide range of mean droplet diameters and droplet size distributions, characterized by a representative Stokes number, based on the droplet arithmetic diameter and the Kolmogorov time scale of the flow, varying between 0.2 and 6, and for turbulent Reynolds numbers of 98, 127, 147, and 235. A novel morphological tracking scheme was used to provide temporal tracking of droplet clusters according to cluster morphological features. The tracking scheme was based on Voronoï space tessellation, multivariate kernel density estimation, and mean shift feature space tracking. The developed tracking scheme was used to establish the relationship between the morphological features of droplet clusters, i.e., number of clusters per unit area and cluster length scales, and the velocity of droplet clusters. The time scale of the droplet clusters increased with both the turbulent Reynolds number and the Stokes number, but its dependence was stronger on the turbulence level. In addition, the effect of filling factors of turbulent flows by turbulent structures on droplet clustering was discussed, which led to suggestions of potential flow control methods to mitigate droplet preferential concentration.

I. INTRODUCTION

In many natural and engineering turbulent two-phase flows, the interaction between turbulence and dispersed droplets results in preferentially concentrated (clustered) droplets, which leads to dense regions, where droplets are more concentrated than the local average value, or voids, where droplets have lower concentration than the local average value. Droplet clustering can significantly affect different engineering applications. For example, the evaporation rate of fuel droplets may be reduced in dense clusters due to the saturation of the surrounding gas by fuel vapour, resulting in local fuel rich regions, which may increase the formation of particulate emissions and reduce combustion efficiency. The increased droplet concentration of droplet clusters can also lead to an increased number of inter-droplet collisions and influence agglomeration in powder production processes. Thus, understanding the mechanism of droplet clustering is essential for optimisation of different engineering applications.

Preferential concentration of mono-sized particles in turbulent flows has been widely studied numerically during the past two decades using Direct Numerical Simulations (DNS). It has been observed that inertial particles are centrifuged in the high strain and low vorticity regions of the flow (Maxey, 1987; Squires and Eaton, 1991; Hardalupas *et al.*, 1990; 1992; Eaton and Fessler, 1994; Wang and Maxey, 1993; and Sundaram and Collins, 1997). However, this mechanism has been argued as incomplete. For instance, in the numerical work of Bec (2005), particles exhibited strong clustering in white-in-time type

flow with the fluid velocity as a given random function of time in the absence of particle centrifuging mechanism. The particle preferential concentration represents a self-similar, multi-scale nature observed both numerically (Boffetta *et al.*, 2004 and Goto and Vassilicos, 2006) and experimentally (Monchaux *et al.*, 2010 and Lian, 2014). The concentrated vorticity at small scales, which is a direct result of the vorticity cascade of turbulent flows, cannot provide a satisfactory explanation for this multi-scale nature of particle concentration.

Strong correlations have been observed numerically between the location of local topological zero acceleration points and the high concentration of inertial particles (Chen *et al.*, 2006; Goto and Vassilicos, 2006; 2008; Bragg *et al.*, 2015; and Sumbekova *et al.*, 2017) since the Radial Distribution Function (RDF) of distances between inertial particles coincide with the RDF of distances between zero acceleration points. To elaborate the observed phenomenon, Goto and Vassilicos (2006) proposed a "sweep and stick mechanism," which suggests that both the local velocity gradient field and inertial particles are swept by the local fluid velocity. The inertial particles stick to and move together with the zero acceleration points and form clusters. In a recent simulation (Bragg *et al.*, 2015), the trajectories of inertial particles were observed to depend upon the interactions with turbulent velocity field at earlier time along their path history. Therefore, the clustering mechanism was "non-local" that does not explicitly depend upon the local flow topology. However, the observed self-similar multi-scale nature of inertial particle clustering remains an outstanding issue that requires explanation.

The parameter that has been used in the above studies to evaluate the relative inertia of the dispersed phase is a particle Stokes number (Crowe *et al.*, 1998), defined as

$$\mathrm{St} = \frac{\tau_p}{\tau_k}, \tag{1}$$

which is the ratio between the particle relaxation time and a specific turbulent time scale. Different studies used different characteristic turbulent flow time scales, but the Kolmogorov time scale is most commonly used for homogeneous, isotropic turbulence, and this is followed in the current paper as well. The particle relaxation time τ_p is defined as

$$\tau_p = \frac{\rho_p D^2}{18\mu}, \tag{2}$$

where ρ_p is the density of a dispersed droplet, D is the droplet characteristic diameter (the arithmetic mean D_{10} is used in this paper), and μ is the fluid dynamic viscosity. According to Eq. (1), very low values of Stokes numbers (i.e., lower than 0.1) indicate high droplet response to flow turbulence.

Despite the availability of a large number of numerical studies, experimental studies remain scarce (Wood *et al.*, 2005; Salazar *et al.*, 2008; Saw *et al.*, 2008; Monchaux *et al.*, 2010; Obligado *et al.*, 2011; and Huck *et al.*, 2018) due to the complexity to conduct two-phase flow experiments. Wood *et al.* (2005) evaluated the effectiveness of the box counting method (Eaton and Fessler, 1994) and two-dimensional Radial Distribution Function (RDF) (Sundaram and Collins, 1997) in quantifying mono-dispersed solid particle preferential concentration within homogeneous and isotropic turbulence with very small mean flow. Strongest particle clustering was observed at flow time scales around 10 times the Kolmogorov time scale, when the corresponding particle Stokes number approaches unity.

Salazar *et al.* (2008) presented measurements of three-dimensional RDF of mono-dispersed solid particle preferential concentration within homogeneous and isotropic turbulence with small mean flow, which were obtained with holographic Particle Image Velocimetry (PIV) and compared to DNS simulations. Saw *et al.* (2008) quantified droplet pair correlations to study clustering of inertial water droplets generated by four spray nozzles in a wind tunnel with a high turbulent Reynolds number. Monchaux *et al.* (2010) proposed Voronoï analysis to quantify preferential concentration of poly-dispersed droplets generated by using an air-assist atomizer in isotropic turbulence with conveying mean flow in a wind tunnel. None of those experimental studies considered the influence of particle/droplet size distribution on preferential concentration. Warhaft (2009) reviewed recent advances in the study of droplet motion and suggested that the droplet size influence should be considered and studied systematically. Bordas *et al.* (2011) presented a study of the influence of turbulence on droplet diameters generated by an air-assist nozzle in spatially decaying turbulence with conveying mean velocity.

However, to the best of our knowledge, all previous studies have focused on the spatial characteristics of droplet clustering, while no experimental investigation of the temporal evolution of poly-dispersed droplet clusters is available. For example, some open questions are as follows: (i) For how long does a droplet cluster survive? (ii) Does the dimension of a droplet cluster affect its time scale? (iii) How does the speed of a droplet cloud in space change? (iv) How does a droplet cloud disperse? Temporal tracking at the scale of coherent clusters may provide new insights and enhance our understanding on the governing mechanism of particle preferential concentration. Baker *et al.* (2017) defined coherent clusters by imposing restriction that clusters are large enough to represent self-similarity based on the Voronoï tessellation and applied it to the distribution of heavy particles in direct numerical simulations. The current paper reports temporal tracking of coherent clusters measured from experiments.

The complexity of turbulent droplet-laden flows and the presence of droplets with a wide range of sizes make the isolation of individual physical mechanisms and associated coupling effects between flow turbulence and droplets difficult. Homogeneous and isotropic turbulence is an ideal flow, which is especially desirable for the study of multiphase flows because of simplifications that can be introduced in the equations. To simplify the experimental investigation of droplet clustering, a volume of homogeneous and isotropic turbulence without a mean flow has been generated and used to study polydispersed droplet dispersion (e.g., Charalampous and Hardalupas, 2010; Lian *et al.*, 2013; and 2017). This flow configuration eliminates the contribution of mean shear and

enables direct comparison with DNS of particle-laden turbulence. It can also allow the evaluation of the effects of polydispersed mean droplet size and the spread of the corresponding size distributions on the formation of droplet clusters, which can occur only due to turbulence without any mean flow contribution.

The paper is organized as follows. Section II describes the experimental setup and the associated high speed imaging system, which records the temporal evolution of the droplet concentration with a temporal resolution approximately one third of the turbulent flow Kolmogorov time scale. Stationary homogeneous and isotropic turbulent flow characterization and poly-dispersed droplet size characteristics are also included in this section. Section III proposes a novel morphological identification and tracking scheme, based on Voronoï space tessellation, multivariate kernel local density estimation, and mean shift feature space tracking. The proposed method provides time-resolved droplet cluster identification and tracking and quantifies the corresponding morphological features. Section IV uses the temporal tracking of droplet clusters, identified by the morphological method proposed in Sec. III and the time and length scales of poly-dispersed droplet clusters. The influence of turbulent flow filling factors, which are explained in this section, leads to suggestions of possible flow control methods to mitigate droplet preferential concentration. Section V summarizes the main findings and proposes future work.

II. EXPERIMENTAL SETUP

Thegeneration of a "volume" of homogeneous, isotropic turbulence without mean flow, known as "Box of Turbulence," was based on the approach of Hwang and Eaton (2004) and Goepfert *et al.* (2009). Charalampous and Hardalupas (2010) and Lian *et al.* (2013) have described the "box of turbulence" used for the current study, and a short description is provided here. Figure 1 shows a photograph of the facility,

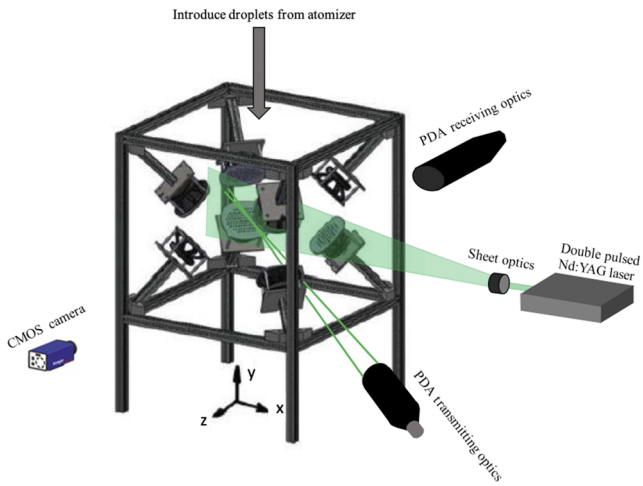

FIG. 1. Experimental setup of "box of turbulence."

which consisted of a cubic frame with 8 loudspeakers placed at the vertices, which are covered by a plate with 50 holes of 8 mm diameter. The loudspeakers operate at a random frequency between 40 Hz and 60 Hz and generate arrays of synthetic jets, which all meet at the centre of the cube. Fine tuning of the amplitude of the imposed oscillations at the loudspeaker membranes allows balancing the flow and generating approximately a 40 mm cubic volume of homogeneous and isotropic turbulence without mean flow at the central region of the experimental facility. Poly-dispersed droplets were introduced from an air-assist atomizer mounted around 1 m above the "box of turbulence" to ensure that droplet momentum is minimum before entering the "box." The droplet size distributions of the associated fully developed sprays were measured by means of Phase Doppler Anemometry (PDA) and could be varied widely by controlling the air and liquid flow rates.

An Edgewave, IS-series, Nd:YAG laser operating at 532 nm was pulsed at a high repetition rate (controllable between 25 Hz and 3 kHz) to generate a planar laser sheet through the centre of the "box." The laser sheet was shaped by a series of cylindrical optics and had a thickness of around 0.1 mm and was aligned at the centre of an illuminated Area of Interest (AOI) of around 45×45 mm^2 at the "box" centre. The laser sheet illuminated the droplets, and the resulting time dependent, instantaneous images of scattered light intensity were recorded at a rate up to 3000 Hz. The air flow characteristics of the "box of turbulence" were measured without the presence of droplets by 2D Particle Image Velocimetry (PIV) with a time lag of 100 μs between the two frames using tracer particles of fine glycol droplets with size less than 3 μm, generated by a VIVID stage fog generator. The instantaneous double frame, double exposure PIV images and the single frame spatial droplet distribution images were captured by using a Photron APX CMOS camera (1024 pixel $\times$ 1024 pixel) with a 105 mm lens f/2.8, leading to a linear magnification of 0.3 and resulting in a spatial resolution of 45.5 μm/pixel. The recording frame rate of the camera for the PIV measurements was set at 1500 Hz, corresponding to a time step of 6.6×10^{-4} s, which represents a time step of around 0.5 times the Kolmogorov time scale, τ_k, of the flow (see Table I). Double-frame, double-exposure image pairs were processed with the PIV software Davis 7.2 from Lavision GmbH to acquire velocity vector fields. The 46.6 mm $\times$ 46.6 mm image pairs were processed twice with an initial interrogation window size of 64 $\times$ 64 with 50% overlap and a final window size of 16 $\times$ 16 with 50% overlap, resulting in a 128 $\times$ 128 vector field. The resulting vector spacing is 364 μm, which is 8 times the spatial resolution of 45.5 μm/pixel of the camera.

A. Turbulent flow characteristics

Four different turbulent intensities were generated by varying the amplitude of the imposed oscillations at the loudspeakers of the experimental setup, leading to turbulent Reynolds numbers Re_λ of 98, 127, 147 and 235, based on the Taylor length scale of the flow. An example of the

TABLE I. Turbulent quantities measured by 2DPIV with a repetition rate of 1500 Hz.

Turbulent quantities	Experiment 1	Experiment 2	Experiment 3	Experiment 4
q^2 (m^2/s^2)	0.441 ± 0.000	0.789 ± 0.002	2.148 ± 0.025	2.262 ± 0.006
ε (m^2/s^3)	4.966 ± 0.085	10.499 ± 0.116	19.692 ± 0.4581	16.151 ± 0.251
λ (m)	0.004 ± 0.000	0.004 ± 0.000	0.004 ± 0.000	0.004 ± 0.000
τ_k (s)	0.003 ± 0.000	0.002 ± 0.000	0.001 ± 0.000	0.001 ± 0.000
η (mm)	0.193 ± 0.000	0.167 ± 0.000	0.134 ± 0.000	0.136 ± 0.000
τ_ς (m)	0.123 ± 0.001	0.122 ± 0.001	0.069 ± 0.000	0.129 ± 0.000
Λ (m)	0.031 ± 0.000	0.039 ± 0.000	0.032 ± 0.000	0.072 ± 0.000
Re_λ	98.854 ± 0.357	126.749 ± 0.440	147.407 ± 0.773	234.888 ± 0.590

spatial distribution of the magnitude of the mean flow velocity, u_{mean}, for a turbulent Reynolds number of 147 is presented in Fig. 2(a) as evaluated from 1024 images, recorded at a rate of 25 Hz. This repetition rate is chosen to ensure sample independence. The velocity magnitude u_{mean} is defined as $\sqrt{u^2+v^2}$, where u and v are the two orthogonal velocity components along the directions x and y determined in Fig. 1, on the plane of the laser sheet. The mean velocity magnitude is less than around 0.1 m/s, approximating zero mean velocity throughout the recorded plane of the flow and establishing stationary turbulence. The spatial contours of the ratio of the velocity fluctuations in the two orthogonal flow directions x and y on the plane of the laser sheet, $\langle \bar{u}_{rms}/\bar{v}_{rms} \rangle$, are presented in Fig. 2(b). The results show that the ratio is bounded between 0.9 and 1.1 and centered around 1 across the recorded plane of the flow. This confirms the spatial isotropy of flow turbulence within the area of interest. The statistical uncertainty of the results of Fig. 2 is estimated to be less than 1% for the mean velocity and around 2% for the velocity ratio, based on a confidence interval of 99%. These results are in agreement with those of other researchers (e.g., Hwang and Eaton, 2004; Goepfert *et al.*, 2009; and Charalampous and Hardalupas, 2010). Appendix A discusses further the evaluation of the isotropy and homogeneity of the turbulent flow.

The time-dependent flow velocity was measured with a repetition rate of 1500 Hz, and the mean flow velocity characteristics are presented in Table II of Appendix A together with the corresponding statistical uncertainties, which are in agreement with the results of Fig. 2, which were obtained at a low sampling rate. The characteristics of the turbulence for all turbulent Reynolds numbers are presented in Table I. The definition of all the parameters and the evaluation method of their values can be found in Appendix A.

B. Poly-dispersed droplet characteristics

An air-assist atomiser, placed at a distance of 1 m above the "box of turbulence," generated sprays with droplets with different mean sizes and spreads of their size distribution, which dispersed through the "box of turbulence." The droplet sizes were controlled by adjusting the inlet water flow rate and supply air pressure at the atomiser. Larger droplet mean diameters were delivered by increasing the water flow rate, while keeping the air pressure constant. The droplet size distributions present in the "box" of turbulence were measured by using a Phase Doppler Anemometry (PDA) system (57 × 80) from Dantec forming an optical focusing probe volume at the centre of the "box of turbulence." The optical setup of the PDA allowed a maximum droplet size of 160 μm to be measured. To acquire sufficient data to describe the droplet size distribution, 5000 validated droplets were measured for each experiment.

The main statistical quantities used to quantify the droplet size are the droplet mean diameters, D_{pq}, droplet number-based diameters, $DN_{x\%}$, representing diameters for different fractions x of the cumulative number of droplets in a size distribution, and droplet volume-based diameters, $DV_{x\%}$, representing diameters for different fractions x of the

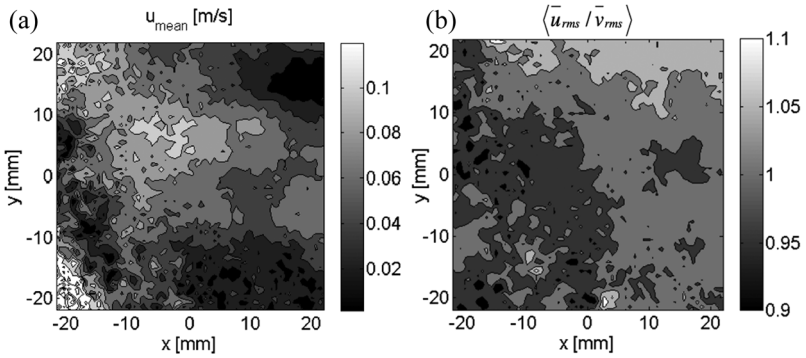

FIG. 2. Spatial contours of (a) mean flow velocity and (b) ratio of r.m.s. of velocity fluctuations in the direction of x and y of the coordinate system of Fig. 1 for the turbulent condition of Re_λ = 147.

cumulative volume of the droplet size distribution. Number-weighted droplet size distributions for different operating conditions of the atomizer are shown in Fig. 3. DN60% is derived from the cumulative droplet number-based size distributions and indicates, respectively, the diameter below which 60% of the total number of droplets in the spray is present. Representative droplet diameters based on a number-weighted size distribution may be more appropriate for scaling the behavior of preferential concentration, which is identified by droplet clusters with large number density and voids with low number density of droplets relative to the average across the imaging region. Volume-weighted size distributions and the corresponding cumulative distributions are also commonly used and are converted from the number-weighted distributions after considering the volume of each droplet size. Representative diameters, DV5%, associated with volume-based size distributions, correspond to diameters below which 5% of the total liquid volume in the spray is present. The droplet size spread is also characterized, according to the volume-based size distribution with a relative diameter span factor (DRSF) defined below (Bayvel and Orzechowski, 1993),

$$\Delta_{DRSF} = \frac{DV_{90\%} - DV_{10\%}}{DV_{50\%}}. \quad (3)$$

Although the droplet size measurements were obtained at the centre of the "box of turbulence," the droplet size distribution remained the same at every location in the "box." This is expected due to the lack of initial droplet momentum when entering the "box." Each measurement represents one set of experiments and is characterized by the droplet Sauter mean diameter D_{32} ranging from 25 μm to 95 μm and droplet arithmetic mean diameter D_{10} ranging from 15 μm to 41 μm. Different size spreads have been achieved and characterized accordingly for each experiment. The representing droplet size and size spread of the size distributions are chosen based on a recent observation that D_{10}, $DV_{5\%}$, and $DN_{60\%}$ are preferable to use for the characterization of droplet clustering in this flow (Lian *et al.*, 2013). The Stokes number is defined by the response time of a droplet with size equal

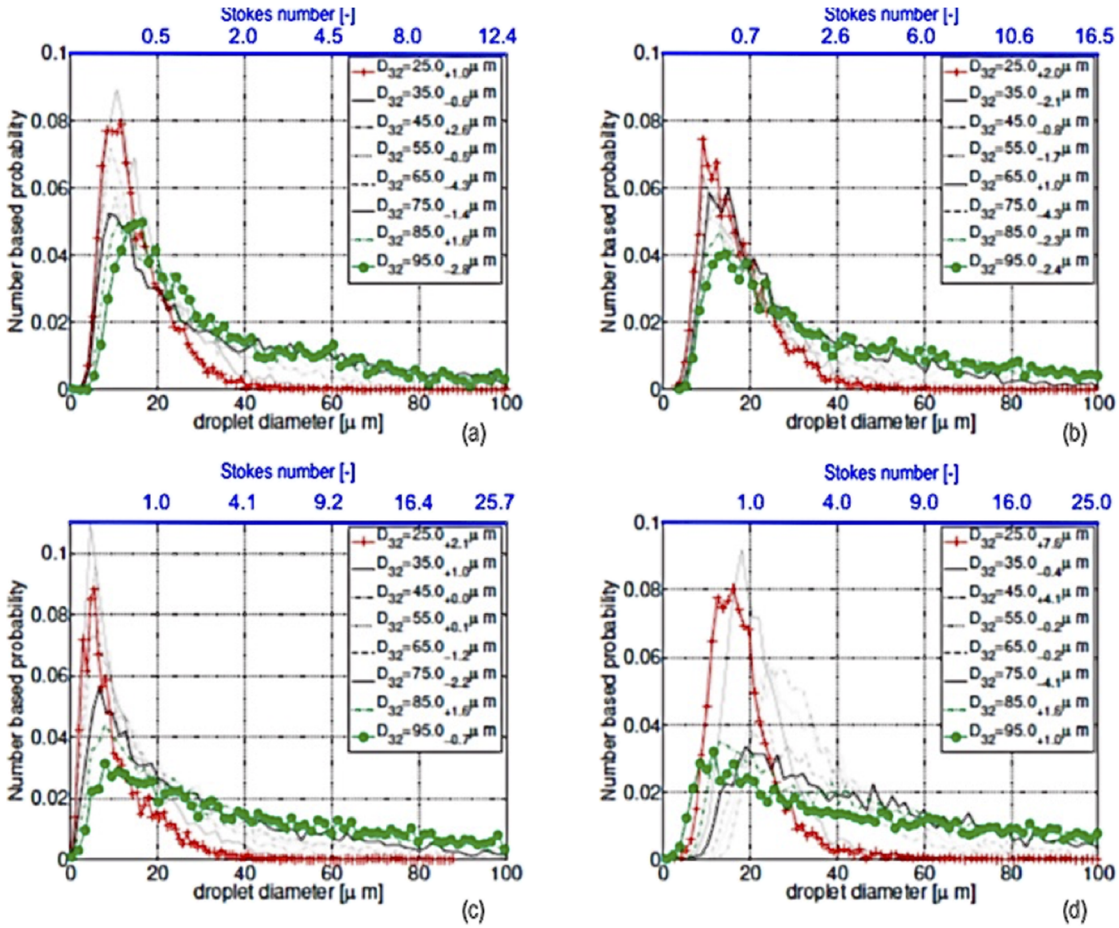

FIG. 3. Number based droplet size distributions of the injected droplets in the 4 turbulent flow conditions with (a) Re_λ = 98, (b) Re_λ = 127, (c) Re_λ = 147, (d) Re_λ = 235.

to the arithmetic mean D_{10}, according to Eq. (1), which is based on the Kolmogorov time scale. A summary of the various representative droplet diameters and droplet size spreads of the considered size distributions is presented in Appendix B. Number based droplet size distributions of the injected droplets for the four turbulent flow conditions are shown in Fig. 3. In the current paper, a representative Stokes number for each droplet size distribution is evaluated based on the arithmetic mean D_{10}. However, the droplet size distributions of Fig. 3 show the range of the Stokes numbers for each flow condition. Figure 3 shows that most of the droplets have Stokes numbers up to around 2. In addition, there is a tendency for the number of the droplets of the size distribution that has Stokes numbers up to around 2 to reduce with the increase in the turbulent Reynolds number. Since the number of droplets, which have the Stokes number larger than 2, is low for all turbulent levels, most of the droplets have similar response to the flow turbulent fluctuations, which may lead to a lower effect of the Stokes number on the droplet clustering.

III. TEMPORAL TRACKING OF DROPLET CLUSTERS

A. Voronoï tessellation

The dimension of the acquired images was 1024 pixel × 1024 pixel with a spatial resolution of 45.5 μm/pixel, which was selected as a compromise between the size of the recorded space on each image and its spatial resolution. As a consequence, there is a possibility that more than one droplet may be present in one pixel. However, given the droplet size distributions of the different cases of the experiment, the probability of such occurrence was low for the low mass loadings of the current experiment. The image recording rate was 3000 Hz. For each experiment with different droplet mean diameters, 1000 raw images of instantaneous light scattering intensity from the droplets were processed based on the image processing method proposed by Lian *et al.* (2013). This method ensured that the droplet locations were identified accurately on each image. The Voronoï analysis decomposes the two-dimensional space into individual Voronoï cells that correspond to each detected droplet with each side of the cell being closer to it than any other droplet. The Voronoï cell area A is the inverse of the local droplet concentration. Thus, the distribution function of Voronoï cell areas can provide information of the instantaneous, local droplet concentration. The distribution function of the normalized Voronoï cell areas A/A_{avg} was applied to the quantification of preferential concentration (Monchaux *et al.*, 2010), and it is also used for the time-dependent measurements of the current study.

The acquired images were recorded in time steps of 3.3×10^{-4} s, corresponding to a recording rate of 3000 Hz, which represents a time step of around $0.3\tau_\kappa$ for the turbulent condition of Re_λ = 147. Figure 4 shows an example of the temporal evolution of droplet dispersion for the droplet size distribution with D_{32} = 55 μm, which includes 8 subsequent frames in time of the Voronoï cells corresponding to the identified droplet centres. The presented frames are 800 pixels × 800 pixels, covering 80% of the area of the acquired experimental images. Image edges were only truncated in this figure to exclude incomplete Voronoï cells and provide better clarity. However, the whole imaging area of 1024 pixels × 1024 pixels was used for all the measurements described in Sec. III B.

In the sequence of 8 presented images of droplet centres with superimposed Voronoi areas of Fig. 4, a droplet cluster is identified by a circle and tracked for the turbulent condition of Re_λ = 147. The initial characteristic length scale of this cluster is approximately 450 μm (100 pixels; equal to 4η) and, after temporal evolution of around 2 ms (equal to $6\tau_\kappa$), merges to a larger cluster and disappears at the fifth frame when the cluster size is reduced to approximately 300 μm (70 pixels; equal to 2η). In the sixth frame, a new larger cluster is formed, probably through merging of the original cluster and another larger cluster, leading to an approximate new cluster size of around 900 μm (200 pixels; equal to 6η). The eighth frame shows that the size of the new cluster reduced to around 670 μm (150 pixels; equal to 4η). It is also clear from Fig. 4 that the shape of the original cluster varies between frames. The behavior of other droplet clusters on the images of Fig. 4 is similar to the one that has been described above.

Itis interesting also to evaluate the velocity of the droplet clusters. It is observed that the circled cluster of Fig. 4 moves both vertically and horizontally in coordinates (x, y) and the displacement is around 225 μm (50 pixels; 1.5η) for the time interval between t_1 and t_6, which is around 2 ms (equal to $1.6\tau_\kappa$), resulting in a velocity of approximately 0.1 m/s, which is similar to the rms of the turbulent velocity fluctuations. The droplets within this cluster appear to move together within the illuminated 2D frame, although some relative motion between individual droplets in the cluster can be observed.

These observations need additional discussion. There are at least two reasons that may change the size and shape of droplet clusters: (i) Droplet clusters have 3D shapes and extend in the normal direction to the laser sheet. The current 2D laser illumination allows only a cross section of a 3D cluster to be visualised. Since the cluster may also move in a direction normal to the laser sheet, the shape of the observed cluster may change due to the change in the visualised cross section of the 3D cluster. (ii) Turbulent dispersion of individual droplets in each cluster may influence the size and shape of the 2D cluster, as droplets disperse relatively to each other. This may be enhanced by the local instantaneous velocity gradient measurements in the turbulent flow.

The observed changes in the cluster size in Fig. 4 have occurred within a time scale of the order of the Kolmogorov scale. This means that the local gas flow did not change within a Kolmogorov time scale, making item (ii) above, related to the turbulent dispersion of the droplets in the cluster, an unlikely source of the observed changes. Therefore, a tentative suggestion is that the changes in the cluster size are probably due to item (i) above, where the inertial out-of-plane

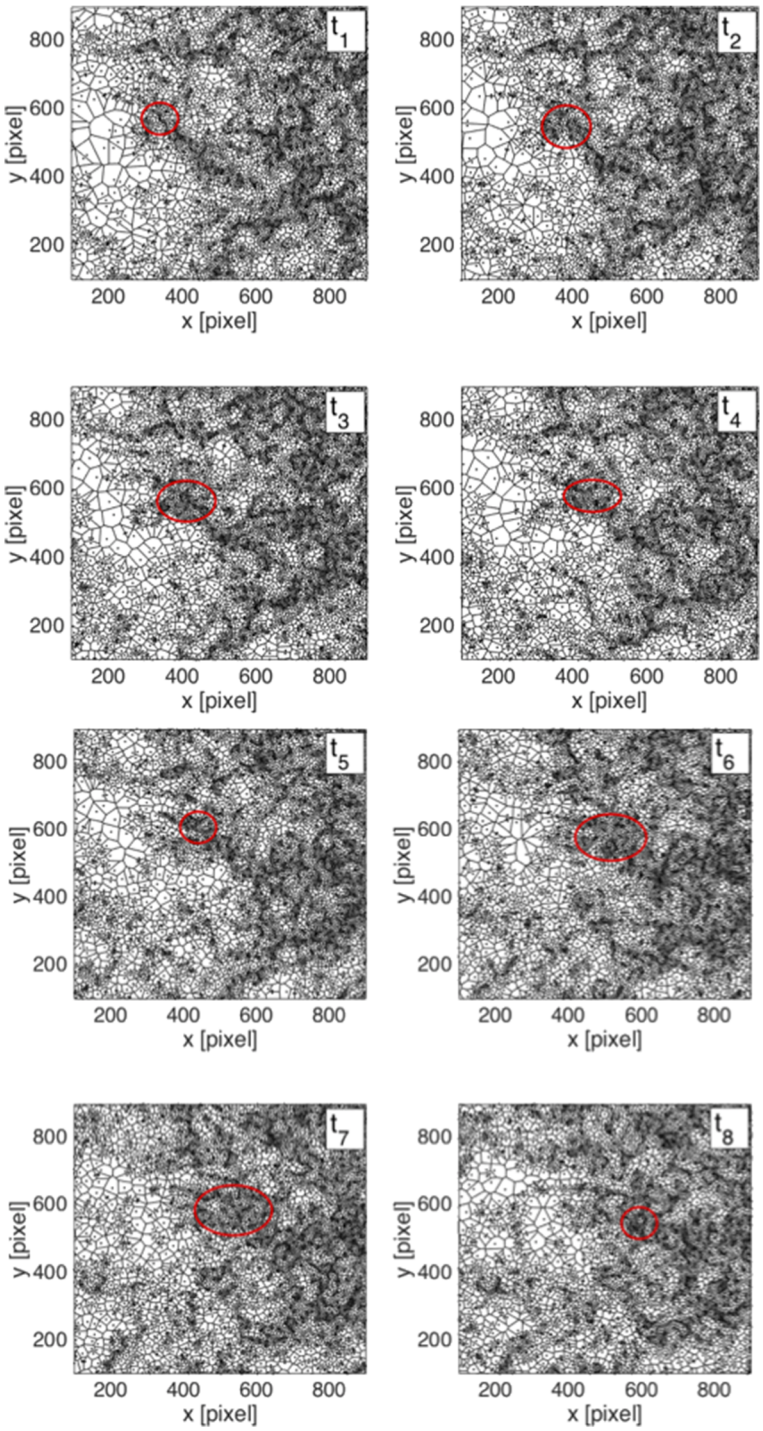

FIG. 4. Example of the temporal evolution of droplet dispersion for the experiment characterized by droplet size distribution with D_{32} = 55 μm for turbulent flow with a Reynolds number of Re_λ = 147. The instantaneous images present the droplet centres and the corresponding Voronoï cells. The time step between images is 3.3×10^{-4} s, which is around 0.3 times the corresponding Kolmogorov time scale.

component of the motion of the clusters, which do not follow faithfully the gas flow, makes the laser sheet to illuminate a different cross section of the cluster. However, further evidence is required for this explanation, which requires the development of a method that can temporally track the 3D droplet clusters to estimate simultaneously the cluster time scale and 3D length scale and shape of the clusters.

B. Cluster identification: Multivariate kernel local density estimation and the modified mean shift analysis

To this end, a novel morphological temporal tracking algorithm is developed to quantify the characteristics of individual droplet clusters, which were detected by visual inspection in Fig. 4. The local droplet number density estimation for the 8 frames of Fig. 4 is illustrated in Fig. 5. As shown in Fig. 5, it is intuitive to identify a "cluster" as the difference in the local density estimation and its gradient. Thus, the developed morphological tracking algorithm introduces Voronoï tessellation to the mean shift feature space analysis widely used for pattern recognition (Comaniciu and Ramesh, 2000 and Comaniciu and Meer, 2002) and can quantify the temporal evolution of the droplet cluster length scale. The mean shift algorithm is a "hill-climbing" algorithm that locates the maxima in the density of sample points by iteratively shifting the multivariate kernel density estimation function at the points of interest to a higher density region until convergence. Traditionally, the points of interest are centres of circular density estimation windows or fixed length grid points. However, the traditional mean shift tracking shares the disadvantages of the quantification methods of box counting and pair correlation, which require *a priori* choice of the fixed grid size leading to ambiguities in identifying droplet clusters, as shown in the previous work of Eaton and Fessler, 1994. Thus,to benefit from the advantages of the Voronoï analysis over the above quantification methods, the mean shift-tracking algorithm is adapted to use the vertices of the Voronoï cells. The combination of the vertices of polygon Voronoï cell as points of interest and the mean shift feature space analysis to identify droplet clusters offers the following advantages: (i) no *a priori* choice of a fixed grid size is required, avoiding the ambiguity in identifying droplet clusters and local density concentration; (ii) each polygon Voronoï cell and its vertices are associated with a single particle at a given time step so that the local droplet density estimation can be developed to identify Lagrangian trajectories of individual droplets and clusters.

The theory of mean shift feature space analysis and its adaptation to include Voronoï space tessellation in identifying and tracking each individual droplet cluster are provided below with detailed discussion on the application of time-resolved droplet cluster identification and tracking.

Given n sample data points x_i, $i = 1, \ldots, n$, on a d-dimensional space, the multivariate kernel density at points of interest $\mathbf{x}$ is estimated (Comaniciu and Meer, 2002) as

$$f(x) = \frac{1}{nh^d}\sum_{i=1}^{n} K\left(\frac{x - x_i}{h}\right), \tag{4}$$

where K is the kernel function and h is the bandwidth parameter of the kernel function. The Gaussian multivariate kernel is one of the most commonly used kernels and is defined (Comaniciu and Meer, 2002) as

$$K(x) = (2\pi)^{-d/2} e^{\left(-\frac{1}{2}\|x\|^2\right)}. \tag{5}$$

The gradient of the density estimation is given (Comaniciu and Meer, 2002) as

$$\nabla f_k(x) = \frac{2}{nh^{d+2}}\sum_{i=1}^{n}(x_i - x)g\left(\left\|\frac{x - x_i}{h}\right\|^2\right)$$
$$= \frac{2}{nh^{d+2}}\left[\sum_{i=1}^{n} g\left(\left\|\frac{x - x_i}{h}\right\|^2\right)\right]\left[\frac{\sum_{i=1}^{n} x_i g\left(\left\|\frac{x-x_i}{h}\right\|^2\right)}{\sum_{i=1}^{n} g\left(\left\|\frac{x-x_i}{h}\right\|^2\right)} - x\right], \tag{6}$$

where $g(x) = -k'(x)$ and k' is the derivative of the kernel function K. The first term of the product of Eq. (6) is proportional to the density estimate at location x. The second term of the product is effectively the mean shift vector $m_{h,G}(x)$, which always points toward the direction of maximum increase,

$$m_{h,G}(x) = \frac{\sum_{i=1}^{n} x_i g\left(\left\|\frac{x-x_i}{h}\right\|^2\right)}{\sum_{i=1}^{n} g\left(\left\|\frac{x-x_i}{h}\right\|^2\right)} - x. \tag{7}$$

The mean shift vector can shift a point of interest $\mathbf{x}$ toward the direction of maximum increase in the density via a path leading to its corresponding centre of "mass." At the centre of mass, the gradient of the density function is zero and the mean shift vector equals zero. In practice, a small arbitrary value is used to define the lower threshold toward zero. This procedure is an adaptive gradient ascent approach. In the regions with low density, the mean shift steps are significantly larger than those in the dense regions. Near the centre of mass, the mean shift analysis is more refined with small shift steps. Note that the mean shift algorithm combined with the Voronoï vertices is slow due to the iterations at each of the vertices.

The steps of the cluster identification procedure based on the mean shift feature space analysis combined with the Voronoï tessellation approach are summarized as follows:

1. The two-dimensional space is divided into Voronoï cells corresponding to each individual droplet. The vertices of polygon Voronoï cells are defined as points of interest for density gradient estimation in the mean shift analysis.
2. Compute the mean shift vector $m_{h,G}(x)$ according to Eq. (7).
3. Shift the points of interest $x^{t+1} = x^t + m_{h,G}(x^t)$ until approaching the centre of mass, where $\nabla f_k(x)$ equals zero, which also yields $m_{h,G}(x)$ equal to zero.
4. The vertices of Voronoï cells that converge to the same "peak" or "centre of mass" are identified as one group of vertices. The droplets contained in complete Voronoï cells in the same vertex group are identified as a droplet cluster. The droplets contained in incomplete Voronoï cells between neighboring clusters are defined as voids.

Based on the mean shift analysis, a "cluster" is identified as droplets with a similar gradient of local number density

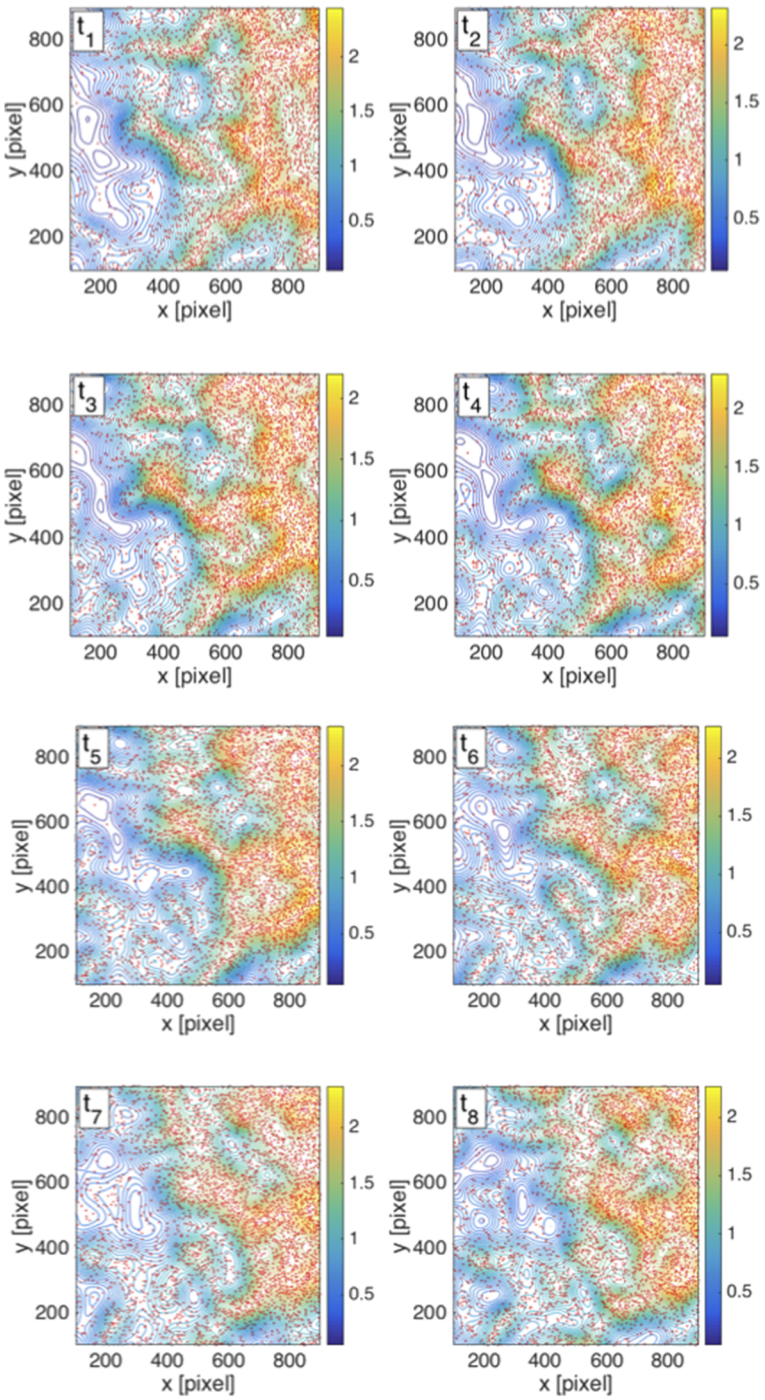

FIG. 5. Example of the temporal evolution of droplet dispersion for the experiment characterized by droplet size distribution with D_{32} = 55 μm for turbulent flow with a Reynolds number of Re_λ = 147. The instantaneous images present the droplet centres and the corresponding local droplet number density estimation. The time step between images is 3.3×10^{-4} s, which is around 0.3 times the corresponding Kolmogorov time scale.

estimation that its Voronoï cell vertices converge to the same centre of mass, as described above. An example of two time consecutive images of the spatial distribution of droplets with a time difference of 3×10^{-4} s is shown in Fig. 6. The clusters are shown in different colors and are observed to move, rotate, transform in shapes, merge, or disappear.

In the process of mean shift feature space analysis, the bandwidth matrix H is the single parameter affecting the outcome of the droplet cluster identification. In the community

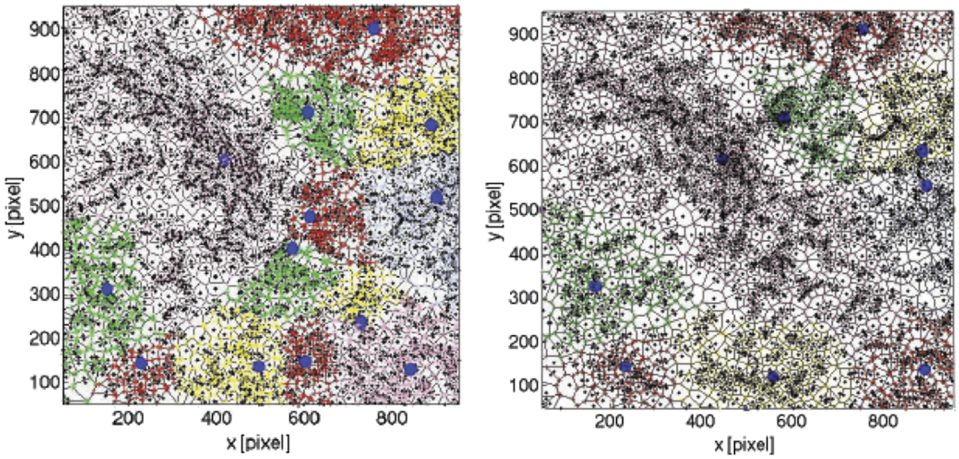

FIG. 6. Droplet cluster identification on two time consecutive images of spatial distribution of droplets.

of pattern recognition, the selection of bandwidth has been commonly assessed empirically (Comaniciu *et al.*, 2001) for tracking objects and is usually characterised by specific color representation histogram. However, the identification of droplet clusters, which have non-rigid shape, requires a more rigorous approach since there is no benchmark histogram to assist the identification process. In the current work, a fixed bandwidth is defined as the optimal bandwidth, which minimises the mean integrated square error (MISE) that achieved the best compromise between the bias and variance in the kernel density estimation and provides optimal global measure of the droplet number density of a sample image. Although kernel density estimation is not required in the mean shift feature space analysis, it has been performed here for the purpose of determining the optimal bandwidth. The mean integrated square error (MISE) (Abramson, 1982) is defined as

$$\mathrm{MISE}(x) = \mathrm{E}\int \left(\hat{f}(x) - f(x)\right)^2 dx, \tag{8}$$

where f(x) is the kernel density estimation function.

For its robustness, the fixed optimal bandwidth is applied for all of the experiments. This suits our purpose of evaluating the spatial and temporal correlations between the identified "clusters" of droplets and stagnation points and avoids the complexity of applying variable bandwidth (Comaniciu *et al.*, 2001) adaptive to the local number density. The time resolved experiments of droplet dispersion are characterised by different turbulent intensities of the flow, droplet size distributions, and number densities. As a result, the optimal bandwidth that minimises MISE is slightly different according to the processed sample image. In order to maintain the consistency of the cluster identification scheme based on the mean shift feature space analysis, the same bandwidth matrix has been used for the processing of all experimental data of spatial droplet distributions. The selection of this "universal" fixed bandwidth matrix is based on the kernel density estimation for the flow condition characterised by droplet size distribution with a Sauter mean diameter D_{32} = 55 μm and droplet spread with a relative diameter span factor of 1.3 for the turbulent flow with a Reynolds number Re_λ = 147.

As explained above, combining the Voronoï tessellation with the mean shift feature space decomposition avoids the effect of fixed grid size so that clusters with non-rigid shape can be identified quantitatively and an equivalent cluster length scale that corresponds to the morphology of the cluster can be defined. Such a cluster length scale l_c is defined as the diameter of a circle that occupies the same area as the non-rigid shaped droplet cluster A_c,

$$\pi\left(\frac{l_c}{2}\right)^2 = A_c, \tag{9}$$

where A_c is the total area of the Voronoï cells defined as one group based on the adapted mean shift analysis.

Cluster identification in the spatial distributions of experimentally determined preferentially concentrated droplets and computationally generated randomly dispersed particles using the mean shift method combined with the Voronoï analysis is shown in Fig. 7. Figures 7(a), 7(c), and 7(e) correspond to the recorded experimental images of preferentially concentrated droplets for the turbulent flow condition of Re_λ = 147. Figure 7(a) shows the identified droplet clusters with the defining Voronoï cell vertices marked with different colors. The droplet clusters with different length scales, as observed from visual inspection, are identified with the centers marked as blue dots in Fig. 7(a). Figure 7(c) shows the corresponding normalized p.d.f. of the Voronoï areas of clustered droplets, which clearly deviates from the Random Poisson Process (RPP) and, therefore, confirms the presence of preferential droplet concentration. Figure 7(e) shows an example calculation of the p.d.f. of cluster length scales averaged over 2048 experimental images with 1024 × 1024 pixels and a spatial resolution of 45.5 μm/pixel. The p.d.f. of the cluster length scales

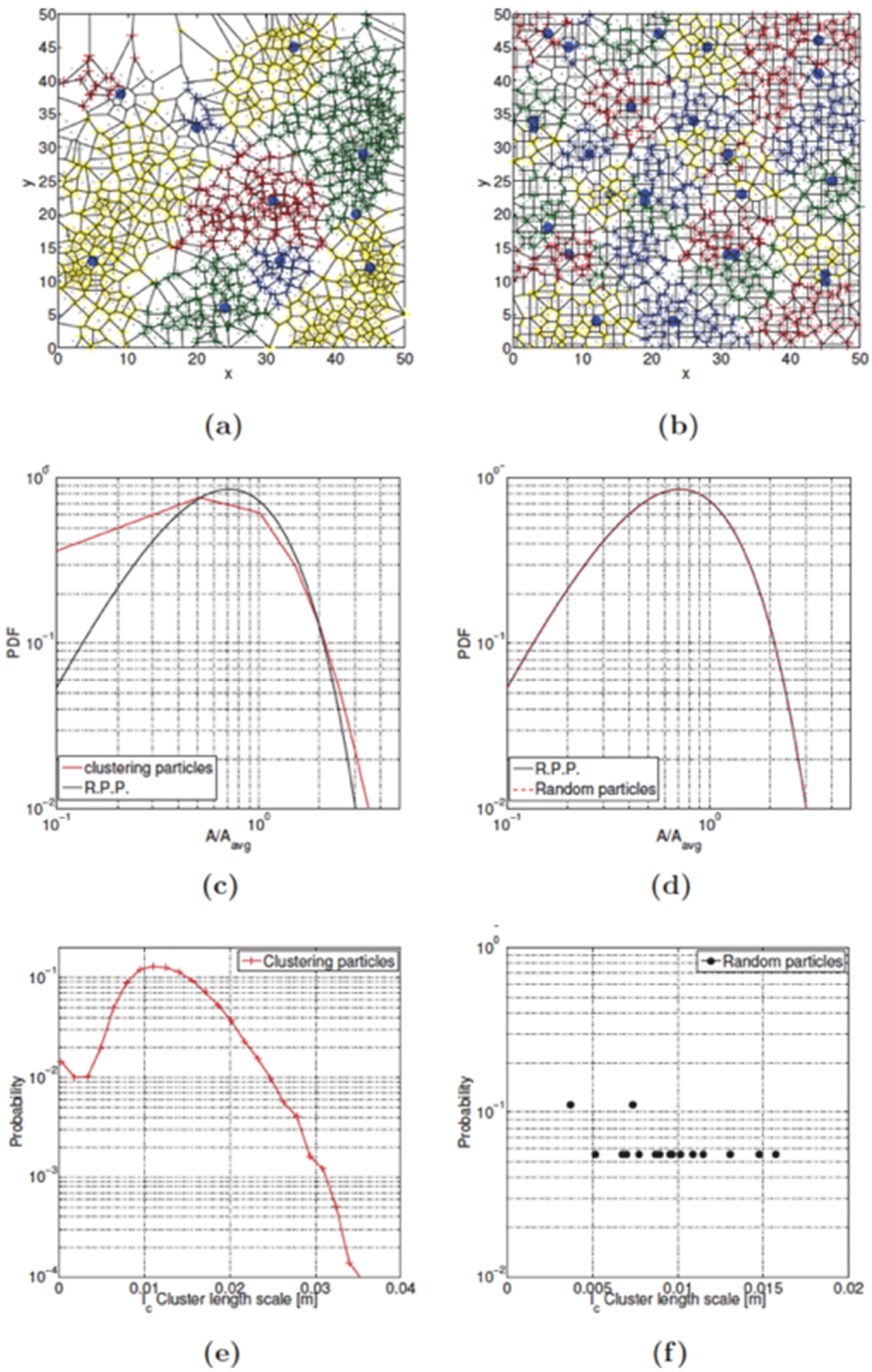

FIG. 7. Droplet cluster identification using the Mean shift method combined with Voronoï tessellation for clustered or random dispersed droplet distributions. Experimental results for clustered droplets for a turbulent flow condition of Re_λ = 147. (a) Example of identified droplet clusters, as indicated by different colors; (c) p.d.f. of normalised Voronoï areas for clustered droplets compared to p.d.f. for randomly distributed droplets; (e) p.d.f. of characteristic length scales of identified droplet clusters. Results for computationally generated random particle distributions: (b) Example of identified clusters for randomly dispersed particles as indicated by different colors; (d) p.d.f. of normalised Voronoï areas for random particle distribution, which agrees with expected shape; (f) p.d.f. of cluster length scales for randomly dispersed particles, which demonstrates similar probability of different length scales.

indicates maximum probability at around 10 mm, suggesting that the most probable droplet cluster length scale for this flow condition is around 10 mm.

Randomly dispersed particles are generated numerically with the same image resolution and domain as achieved in the experiment. The developed cluster identification method is examined by processing those randomly distributed particles. It is expected that no particular cluster length scales would be identified preferentially in the generated distributions. Figure 7(b) shows the identified pseudo-clusters

with the defining Voronoï cell vertices marked with different colors. It appears that these pseudo-clusters have similar length scales. Figure 7(d) shows the normalized p.d.f. of Voronoï areas of randomly distributed droplets that coincides with the random Poisson process well, as expected. Figure 7(f) shows the p.d.f. of the cluster length scales of randomly distributed particles averaged over 1500 sample realizations. The distribution of cluster length scales spreads over a wide range with similar probability, and no higher probability is observed for some length scales, which is clearly different from the case of preferential concentration shown in Fig. 7(e). This demonstration provides confidence in the developed droplet cluster identification method.

IV. TIME SERIES ANALYSIS OF DROPLET NUMBER DENSITY SPATIAL DISTRIBUTIONS

This section presents the characteristics of droplet preferential concentration in the "box of turbulence," as quantified by the Voronoï analysis and the modified mean shift algorithm. The goal here is to evaluate the magnitude of droplet clustering and the effect of turbulent flow characteristics on the typical cluster time scales and length scales.

A. Time scale of droplet clusters

The temporal correlation in the evolution of the standard deviation of the normalized Voronoï areas is evaluated by the auto-correlation coefficient function, defined in Eq. (10),

$$\rho(\tau) = \frac{\langle \sigma_v'(t)\sigma_v'(t+\tau)\rangle}{\langle \sigma_v'^2(t)\rangle}. \tag{10}$$

Note that the mean value of the standard deviation of normalised Voronoï areas has been subtracted, so the fluctuating component of the standard deviation $\sigma_v' = \sigma_v - \overline{\sigma}_v$ is used for the calculation of the auto-correlation coefficient function. The auto-correlation coefficient function of the time dependent fluctuations of the standard deviation of the normalised Voronoï areas is presented in Fig. 8 for different droplet size distributions, which have different representative Stokes numbers, as indicated in Table III, for the four turbulent flow conditions of Re_λ = 98, 127, 147, 235. The time

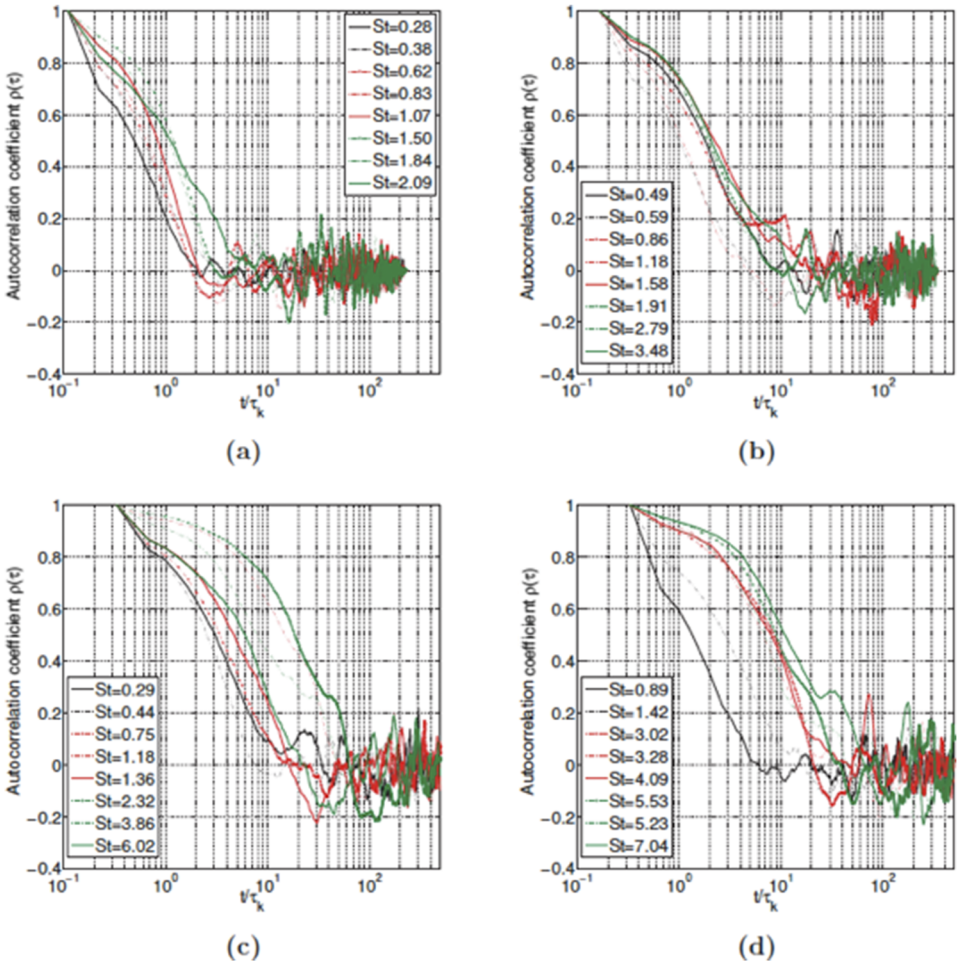

FIG. 8. Auto-correlation coefficient function of the fluctuations of the standard deviation of the normalized Voronoï areas for the four turbulent flow conditions of (a) Re_λ = 98, (b) Re_λ = 127, (c) Re_λ = 147, and (d) Re_λ = 235 and for a wide range of droplet Stokes numbers. Time is normalized by the corresponding Kolmogorov time scale of the flow.

scale of the droplet clusters is represented by the time when the auto-correlation coefficient function becomes zero for the first time. Figure 8 shows that for the four flow conditions, the time scale of the droplet clusters is in the range of 2×10^0 and 8×10^1 times the Kolmogorov time scale and, for most conditions, is close to 10^1. A consistent trend for all turbulent flows is that the cluster time scale is lower for the droplet size distributions with the lower Stokes number. There is an increase in the cluster time scale by around a factor of 3 to 4 over a change of 10 times of the Stokes number. An increase in the turbulent Reynolds number leads to an increase in the cluster time scale, which is around 10 times over an increase in the turbulent Reynolds number by a factor of 2.5. Therefore, the results show that the effect of the turbulent Reynolds number is larger than the effect of the Stokes number on the cluster time scale. This may suggest that droplet clustering is more intense for higher level of turbulence. Such a behavior has been observed by DNS (Tagawa *et al.*, 2012) and experiments (Obligado *et al.*, 2011). In addition, Sumbekova *et al.* (2017) also concluded that the turbulent Reynolds number had a more dominant role than the Stokes number. The current experiment does not have a mean flow, while the experiments of Sumbekova *et al.* (2017) included a mean flow. Therefore, the results suggest that the effect of the mean flow does not affect the qualitative behavior of droplet clustering.

B. Droplet cluster tracking: Mean shift based droplet identification

The probability distributions of the number of identified droplet clusters on the area of the recorded images for all droplet size distributions and for the four turbulent flows with Reynolds numbers Re_λ = 98, 107, 127, and 235 are shown in Fig. 9. The results show that the most probable number of clusters is 10 per image for all experimental conditions. The physical dimensions of each image are 45 mm × 45 mm. This suggests that the most probable number of turbulent flow structures that can lead to the formation of droplet clusters is also around 10 in an area of 45 × 45 mm^2 in the "box of turbulence."

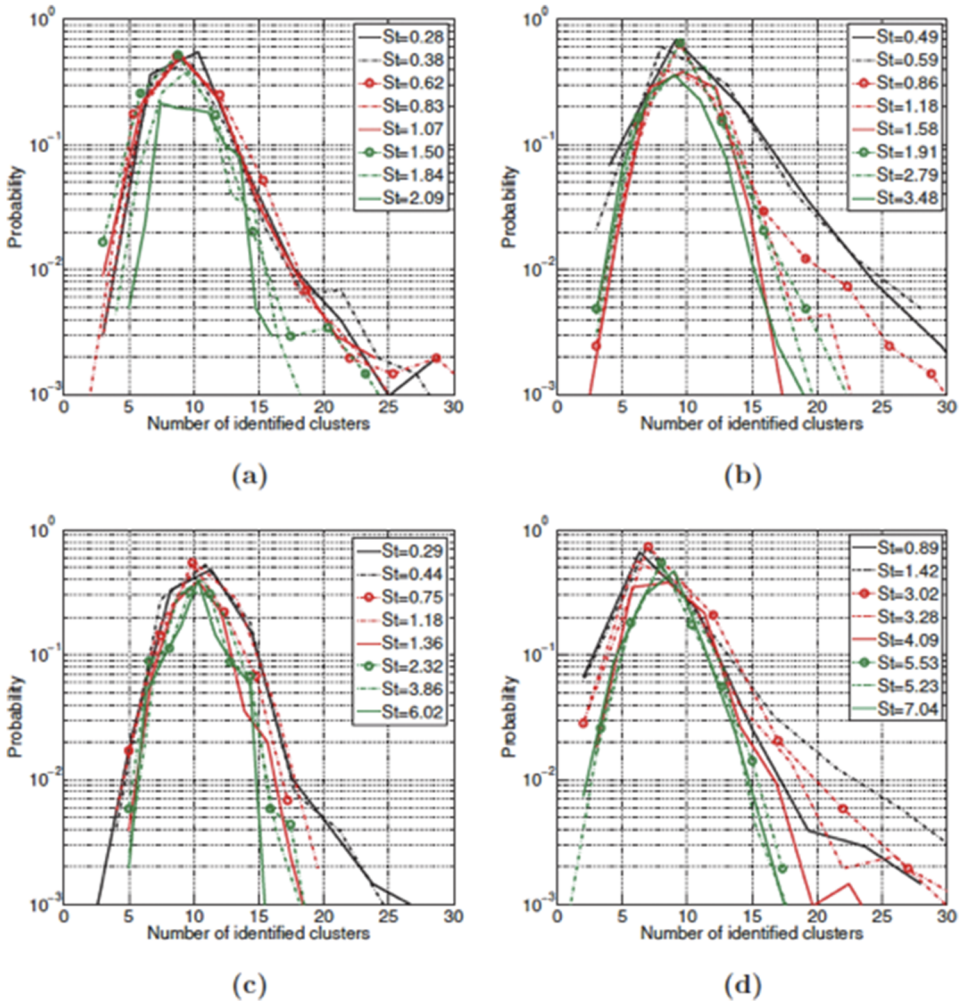

FIG. 9. P.d.f.s of the number of identified droplet clusters in an area of 45 × 45 mm^2 of the homogeneous, isotropic turbulent flow for the four turbulent flow conditions (a) Re_λ = 98, (b) Re_λ = 127, (c) Re_λ = 147, and (d) Re_λ = 235 and for different droplet Stokes numbers.

To illustrate the relationship between the number of identified droplet clusters per image area and the magnitude of droplet clustering, the average number of identified droplet clusters is correlated to the standard deviation of the normalized Voronoï areas in Fig. 10 for all four turbulent flow conditions and for all Stokes numbers detailed in Table III. It is shown that the average number of droplet clusters decreases with the increase in the magnitude of droplet clustering. This is expected since a larger number of droplets form a cluster when the magnitude of droplet clustering is higher and the total number of droplets captured in each frame is approximately the same, as determined by the number of droplets that are supplied to the flow. The established relationship between the number of identified droplet clusters and the magnitude of droplet clustering may be useful for the design of a flow control device aiming to mitigate the magnitude of droplet clustering for various applications.

The instantaneous cluster length scale can also be calculated by using the newly developed cluster tracking method for all droplet conditions and for the four turbulent flows. The p.d.f.s of the droplet cluster length scale [defined according to Eq. (9)] for each measurement condition are based on 2048 images and are plotted in Fig. 11. The most probable cluster length scale is between 10 and 100 Kolmogorov length scales η and tends to increase from around 50-60η for low turbulent levels to around 80-90η for high levels of turbulence. The p.d.f.s of Fig. 11 show that the length scales of the droplet clusters can vary between values below 10 times the Kolmogorov length scale up to values around 300 times the Kolmogorov length scale. This information is presented experimentally for the first time. This shows that the droplet cluster size can be affected by flow structures with a wide range of length scales since the droplet clusters are expected to occur due to interactions with the turbulent flow. Therefore, it is interesting to consider the structures with similar length scales in the turbulent flow.

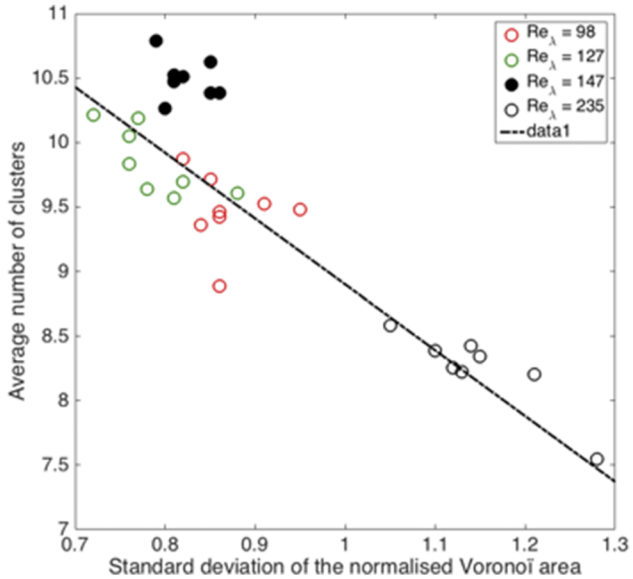

FIG. 10. Relationship between the temporal average of the standard deviation of the normalized Voronoï areas and the average number of identified clusters per image area of 45 × 45 mm^2 for the four turbulent flow conditions with Re_λ = 98, 127, 147, and 235 and the droplet Stokes numbers detailed in Table III.

In Fig. 11, high probability is also observed for formation of small clusters with length scales below 10η, as well as clusters with length scales larger than 50η. These observations suggest that there are variations in the mechanism of droplet cluster formation. The correlation between the number of droplet clusters and the normalized cluster length scales, measured from 2048 images, and a constant droplet size distribution with D_{32} = 55 μm for the four turbulent conditions, is illustrated as scatterplots in Fig. 12(a). Figure 12(a) confirms that the cluster length scale is smaller when the number of clusters per image is larger. There is an approximate linear relationship between the number of droplet clusters and the corresponding length scale, which is not dependent on the droplet Stokes number; thus, only the scatterplot for one size distribution with D_{32} = 55 μm is presented as an example. Larger cluster length scales are observed when the turbulent Reynolds number is higher. This suggests that the relationship between the number of droplet clusters and their length scales is mainly affected by the turbulent flow structure, i.e., the number of turbulent flow structures present per unit flow area (or filling factor of the flow by turbulent structures), which must be responsible for the change in the number of droplet clusters present in the droplet spatial distribution.

The relationship between the normalized mean cluster length scale and the total area occupied by droplet clusters, defined as the sum of the areas of complete Voronoï cells corresponding to the total number of droplets present in clusters, is shown in Fig. 12(b). The total area occupied by clusters increases for larger cluster length scales and reaches a plateau when the average droplet cluster length scale approaches 10^2 Kolmogorov length scales. In agreement to the correlation between the number of droplet clusters and the normalized cluster length scales, the relationship between the total area occupied by droplet clusters and the averaged cluster length scale is independent from the droplet Stokes number and mainly affected by the turbulent flow. This finding suggests that the spatial separation of droplet clusters can affect the variation in the length scale of droplet clusters, the number of droplet clusters, and eventually the magnitude of droplet clustering. Thus, it may be possible to find a flow control method to modify the length scale of droplet clusters, formed during preferential concentration, as a method to mitigate the magnitude of droplet clustering.

The developed droplet cluster identification method enables the temporal tracking of droplet clusters. The displacement of the droplet cluster centres and the local density estimation are illustrated in Fig. 13 for 8 consecutive frames. It shows that the identified droplet clusters move, rotate, transform in shape, merge, or disappear. Thus, it is difficult to calculate quantitatively the velocity magnitude and the vector angle of the droplet cluster centre. However, the ratio of the droplet cluster length scale to the corresponding time

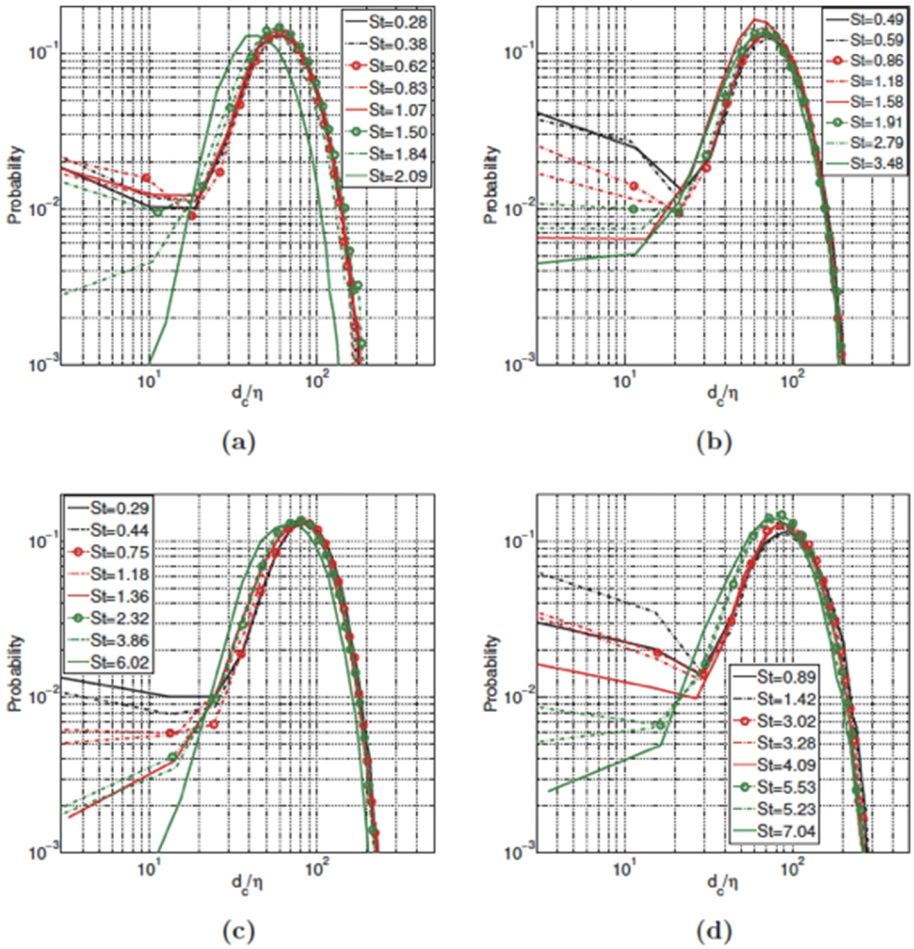

FIG. 11. P.d.f.s of the length scale of the identified droplet clusters for the four turbulent flow conditions (a) Re_λ = 98, (b) Re_λ = 127, (c) Re_λ = 147, and (d) Re_λ = 235 and for different droplet Stokes numbers.

scale provides a characteristic velocity of droplet clusters. The time scale of droplet clusters was found to be in the range of 10^1 to 10^2 times the Kolmogorov time scale in Sec. IV A. As shown in Fig. 11, the cluster length scale is in the range of 10^1 to 10^2 times the Kolmogorov length scale. Thus, the velocity of droplet clusters is in the range of 10^1 m/s, which is similar to the turbulent flow velocity fluctuations.

According to the findings in the literature, the typical average droplet cluster radius is in the range of 20 to 30 times the Kolmogorov length scale, which is effectively 40

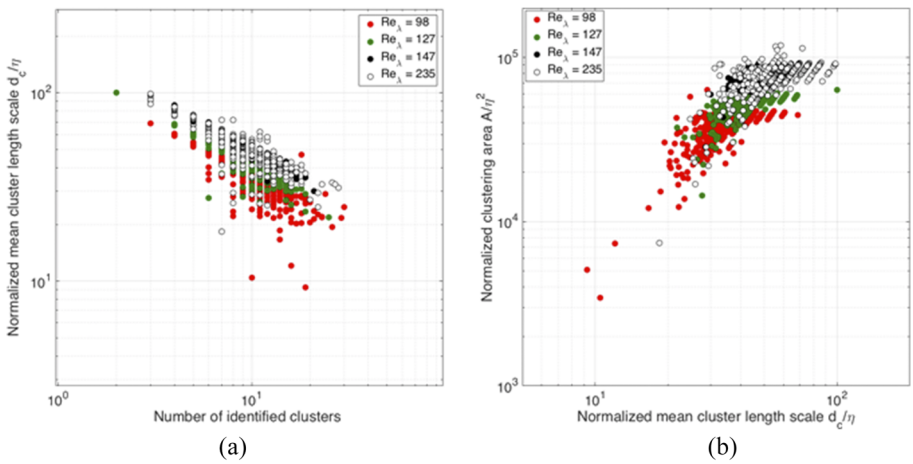

FIG. 12. Correlation between the number of droplet clusters and their length scales for droplet size distribution with D_{32} = 55 μm corresponding to St = 1.18 for turbulent flows with Re_λ 98, 127, 147, and 235, based on 2048 images of instantaneous droplet spatial distributions. (a) Average number of identified clusters per image area and average cluster length scale. (b) Average number of identified clusters per image area and average clustering area. The image area is 45 × 45 mm^2.

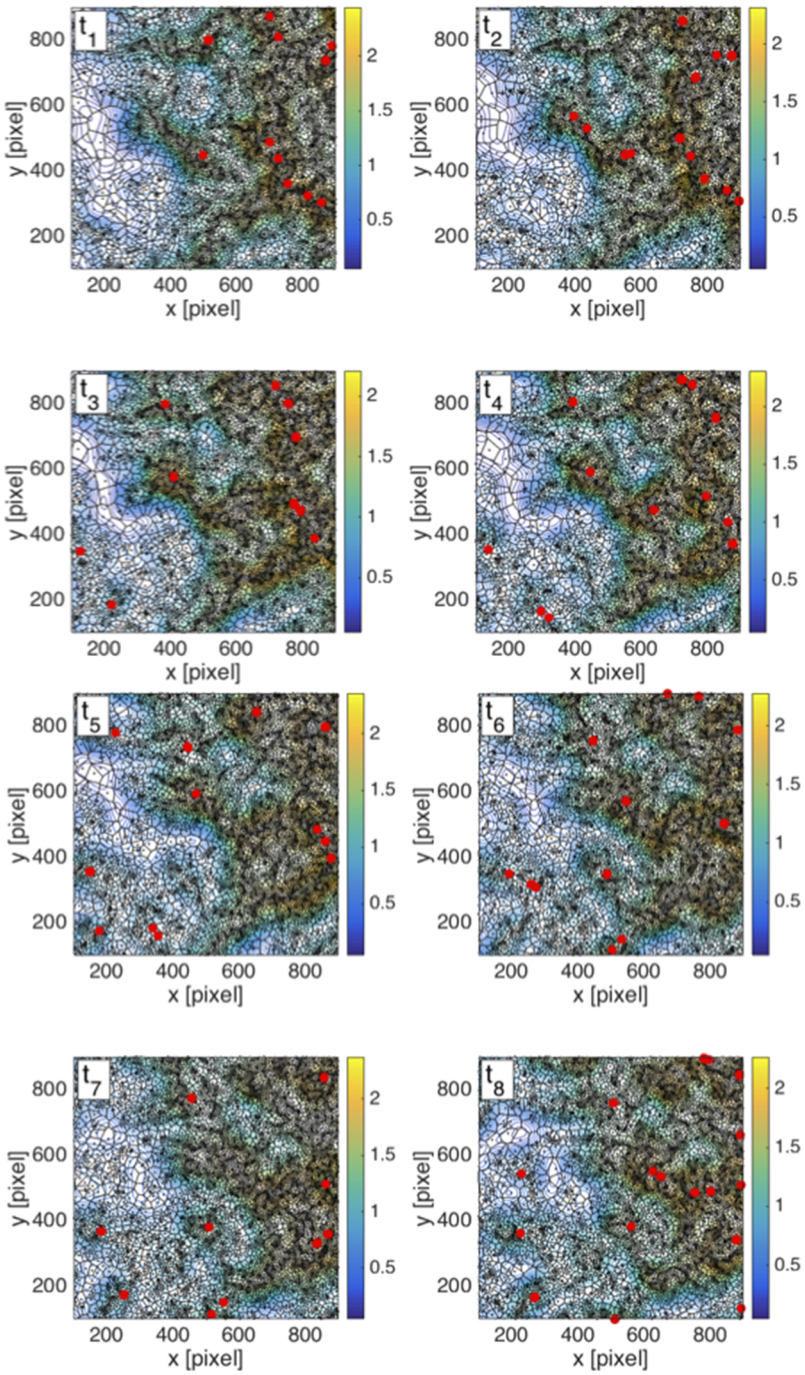

FIG. 13. Example of the temporal evolution of droplet clusters for the experiment characterized by droplet size distribution with D_{32} = 55 μm for a turbulent flow Reynolds number Re_λ = 147 (droplet Stokes number = 1.18). The instantaneous images present the droplet locations, the corresponding Voronoï cells, and the identified cluster mass centre. The time step between images is 3.3×10^{-4} s, which is around 0.3 times the corresponding Kolmogorov time scale.

to 60 times the Kolmogorov length scale if viewed as the equivalent diameter of the droplet clusters. The results on the cluster length scale, based on two entirely different approaches, agree reasonably well.

In summary, the temporal evolution of the standard deviation of the normalized Voronoï areas was analyzed, which quantified experimentally measured temporally resolved poly-dispersed droplet clustering in homogeneous and isotropic turbulence without mean flow. In agreement with previous findings in the literature, the most probable time scale of poly-dispersed droplet clusters is in the range of 10^1 times the Kolmogorov time scale. The morphological characteristics of droplet clustering were quantified by a proposed pattern recognition method, combining Voronoï

tessellation and kernel density estimation. It has been found that the droplet cluster area and length scale increased with higher magnitude of preferential concentration, while the number of clusters decreased. Thus, it may be possible to find a flow control method to modify the length scale of droplet clusters, formed during preferential concentration, as a method to mitigate the magnitude of droplet clustering. With the pattern recognition method, the velocity of droplet clusters was estimated to be in the range of 10^1 m/s, similar to the turbulent flow velocity fluctuations.

V. CONCLUSIONS

Time dependent measurements of the spatial distribution of droplet concentration were obtained for a wide range of droplet size distributions, characterized by a representative Stokes number, based on the droplet arithmetic diameter and the Kolmogorov time scale of the flow, varying between 0.2 and 6, in a "box" of homogeneous and isotropic turbulence with turbulent Reynolds numbers of 98, 127, 147, and 235 without mean flow. The droplet preferential concentration was quantified by two-dimensional Voronoï tessellation, and the temporal evolution of droplet clusters was quantified by a newly developed morphological tracking algorithm. The effect of filling factors of turbulent flows by turbulent structures on droplet clustering characteristics is discussed, with cluster length scale defined by the proposed morphological tracking algorithm, which leads to suggestions of potential flow control methods to mitigate the droplet preferential concentration. The main findings are listed below.

(1) A novel morphological temporal tracking algorithm was developed to identify and track individual droplet clusters in time. The mean shift-tracking algorithm is adapted using the vertices of the Voronoï cells, instead of the grid vertices. Defining vertices of polygon Voronoï cells as points of interest required a major development in order to adopt the mean shift feature space analysis in identifying droplet clusters with several advantages: (i) no "*a priori*" choice of a fixed grid size is required, thus avoiding the ambiguity in identifying droplet clusters and local density concentration; (ii) each polygon Voronoï cell and its vertices are associated to a single droplet at a given time step so that the local number density estimation can be developed to perform Lagrangian tracking of droplets and droplet cluster trajectories.

(2) Analysis, based on the developed mean shift-tracking algorithm, quantified the temporally and spatially averaged cluster length scales to be in the range of 40η to 50η for all the considered droplet size distributions. The relationships between the identified number of droplet clusters, its length scale, and the total "clustering area" were evaluated. It was found that, in agreement with the correlation between the number of droplet clusters and the normalized cluster length scales, the relationship between the total clustering area and the averaged cluster length scale was independent of the droplet Stokes number and mainly affected by the level of turbulence in the flow. This finding suggests that the spatial separation of the clusters can affect the variation of the length scale of droplet clusters, the number of droplet clusters per unit flow area, and eventually the magnitude of droplet clustering. Thus, devising a flow control method to modify the length scale of droplet clusters and the corresponding filling factor of the associated space during preferential concentration can lead to a method to mitigate the magnitude of droplet clustering.

(3) The time scale of the droplet clusters is in the range of 2×10^0 and 8×10^1 times the Kolmogorov time scale and, for most conditions, is close to 10^1. A consistent trend for all turbulent flows is that the cluster time scale is lower for the droplet size distributions with the lower Stokes number. There is an increase in the cluster time scale by around a factor of 3 to 4 over a change of 10 times of the Stokes number. An increase in the turbulent Reynolds number leads to an increase in the cluster time scale, which is around 10 times over an increase in the turbulent Reynolds number by a factor of 2.5. Therefore, the results show that the effect of the turbulent Reynolds number is larger than the effect of the Stokes number on the cluster time scale.

(4) Droplet clusters were observed to move, rotate, transform in shapes, merge, or disappear. Thus, it is difficult to quantify the temporal evolution of the velocity of individual droplet clusters. The velocity of droplet clusters was evaluated both as the ratio between the most probable droplet cluster time scale and length scale and by visual inspection of the vector displacement of the mass centre of the identified clusters. The velocity of droplet clusters was measured to be comparable to the turbulent velocity fluctuations.

ACKNOWLEDGMENTS

The authors would like to acknowledge financial support from the Engineering and Physical Sciences Research Council (EPSRC) under Grant No. EP/E029515/, the European Union COST Action No. MP0806, and the National Natural Science Foundation of China (NSFC) under Grant No. 1187020923.

APPENDIX A: FLOW CHARACTERISTICS

The time-dependent flow velocity was measured with a repetition rate of 1500 Hz, corresponding to a time step of 6.6×10^{-4} s, which represents a time step of around $0.5\tau_k$. The mean flow velocity and the corresponding velocity fluctuations along the x and y directions for the four flow conditions are summarised in Table II with the corresponding uncertainties, which are estimated based on a confidence interval of 99%. The average velocity in both directions is close to zero, suggesting that the mean flow velocity is negligible for all four turbulent flow conditions, in agreement with the non-temporally resolved measurements of Fig. 2.

Both one-dimensional and two-dimensional turbulent kinetic energy spectra were calculated from the measured PIV vector maps to confirm that the flow is homogenous and isotropic. The one-dimensional energy spectrum was defined based on the corresponding two-point correlation functions (George, 2006),

$$F_{i,j}^{(1)}(k) = \frac{1}{2\pi}\int_{-\frac{T}{2}}^{+\frac{T}{2}} e^{-ikr} B_{i,j}(r,0,0)dr, \tag{A1}$$

where the two-point correlation function is defined as

$$B_{i,j}(\vec{r},t) = \int_{-\frac{T}{2}}^{+\frac{T}{2}} \left\langle \hat{u}_i\left(\vec{k'},t\right)\hat{u}_j^*\left(\vec{k},t\right)\right\rangle e^{i(k'_m - k_p)}d\vec{k}\int_{-\frac{T}{2}}^{+\frac{T}{2}} d\vec{k'}. \tag{A2}$$

The calculation procedure started by subtracting the temporal mean flow velocity and then performing fast Fourier transform (FFT) of the fluctuating velocities at each row of the velocity vector map and averaging over all the images. The universal Kolmogorov spectrum (Kolmogorov, 1941) is defined as

$$E_{\alpha\alpha}(k_\alpha) = \frac{18}{55}C_k(\varepsilon)^{\frac{2}{3}}(k_\alpha)^{-\frac{5}{3}}, \tag{A3}$$

where C_k is the constant determined as 1.5 by Pope (2000). k_α is the wavenumber defined as

$$\overrightarrow{k_\alpha} = \frac{2\pi}{\overrightarrow{r_\alpha}}, \tag{A4}$$

where ε is the turbulent dissipation rate, calculated with the direct method described by Jong *et al.* (2008) under the assumptions of homogeneity and isotropy. The one dimensional kinetic energy spectrum is presented in Fig. 14(a). The turbulent flow is considered isotropic, following the energy spectrum collapse on longitudinal and transverse directions and the relationship between longitudinal and transverse spectra agreeing with the suggestion of Monin and Yaglom (1971) as

$$E_{\alpha\alpha}(k_\alpha) = 0.75E_{\beta\beta}(k_\alpha). \tag{A5}$$

The deviation from the –5/3 slope at high wavenumbers is an artifact of the measurement method and has been observed by other researchers (Hwang and Eaton, 2004 and Goepfert *et al.*, 2009). This is probably due to remaining noise on the velocity measurements and the increased spacing between the PIV velocity vectors, and this effect becomes more important at high wavenumbers. Non-temporally resolved 2D PIV measurements confirmed the influence of above sources on the resulting spectra (Charalampous and Hardalupas, 2010). Therefore, the good agreement in both longitudinal and lateral kinetic energy spectra supports the isotropy of turbulence. The two-dimensional kinetic energy spectrum was also calculated from the squared one-dimensional spectrum in longitudinal and lateral directions and is shown in Fig. 14(b).

TABLE II. Average turbulent velocity measured by 2DPIV with a repetition rate of 1500 Hz.

No. of experiments	Experiment 1	Experiment 2	Experiment 3	Experiment 4
$\langle\bar{u}\rangle$ (m/s)	−0.016 ± 0.000	−0.022 ± 0.000	0.049 ± 0.000	0.028 ± 0.001
$\langle\bar{v}\rangle$ (m/s)	−0.018 ± 0.000	0.072 ± 0.000	−0.001 ± 0.000	0.064 ± 0.001
$\langle\bar{u}_{rms}\rangle$ (m/s)	0.384 ± 0.000	0.505 ± 0.001	0.746 ± 0.003	0.866 ± 0.001
$\langle\bar{v}_{rms}\rangle$ (m/s)	0.380 ± 0.000	0.512 ± 0.001	0.734 ± 0.003	0.849 ± 0.001

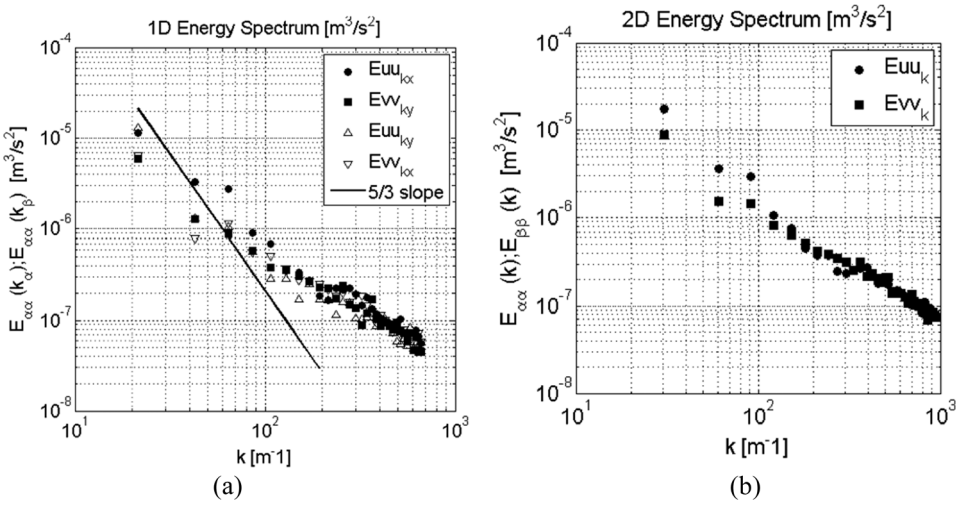

FIG. 14. 1D and 2D kinetic energy spectra for the turbulent condition of Re_λ = 147.

Other turbulent scaling quantities were calculated based on the dissipation rate with the following definitions. The estimated characteristics of turbulence in the current flow condition are presented in Table I. The turbulent kinetic energy is defined as

$$q^2(x,y) \cong 3\frac{u_{1,rms}^2(x,y) + u_{2,rms}^2(x,y)}{2}. \tag{A6}$$

The Reynolds number, associated with the Taylor microscale, is

$$\mathrm{Re}_\lambda \cong \frac{\overline{\lambda(q^2/3)^{1/2}}}{\nu}, \tag{A7}$$

where ν is the kinematic viscosity of the air, which is 1.57×10^{-5} m^2/s at atmospheric pressure and temperature, and λ is the Taylor microscale defined as

$$\lambda \cong \overline{\left(\frac{5\nu q^2}{\varepsilon}\right)^{\frac{1}{2}}}. \tag{A8}$$

The Kolmogorov time and length scales, τ_k and η, are, respectively, defined as

$$\tau_k \cong \overline{\left(\frac{\nu}{\varepsilon}\right)^{\frac{1}{2}}}, \tag{A9}$$

$$\eta = \overline{\left(\frac{\nu^3}{\varepsilon}\right)^{\frac{1}{4}}}, \tag{A10}$$

$$\eta = \overline{\left(\frac{\nu^3}{\varepsilon}\right)^{\frac{1}{4}}}. \tag{A11}$$

APPENDIX B: DROPLET CHARACTERISTICS

TABLE III. Characteristics of dispersed droplets in the considered turbulent flows. Diameter unit in microns.

Exp. no	D_{10}	D_{32}	$DN_{40\%}$	$DN_{60\%}$	$DV_{5\%}$	$DV_{50\%}$	Δ_{DRSF}	$St_{D_{10}}$
Re_λ = 97								
No. 1	15.0	25.0 + 1.0	10.8	14.3	11.9	28.3	1.7	0.28
No. 2	17.5	35.0 − 0.6	11.9	16.3	14.8	39.4	1.9	0.38
No. 3	22.4	45.0 + 2.6	13.7	20.4	21.8	56.6	1.2	0.62
No. 4	25.9	55.0 − 0.5	15.0	23.6	26.5	63.6	1.0	0.83
No. 5	29.3	65.0 − 4.3	16.4	26.7	30.8	70.7	0.9	1.07
No. 6	34.7	75.0 − 1.4	18.6	32.4	39.0	86.6	0.8	1.50
No. 7	38.5	85.0 + 1.6	20.3	34.2	43.4	105.0	0.8	1.84
No. 8	41.0	95.0 − 2.8	22.0	35.3	46.7	116.5	0.7	2.09
Re_λ = 127								
No. 1	17.1	25.0 − 2.0	12.6	14.8	13.4	30.4	1.4	0.49
No. 2	18.8	35.0 − 2.1	13.3	18.2	15.6	37.2	1.4	0.59
No. 3	22.7	45.0 − 0.8	15.0	21.2	20.1	51.8	1.2	0.86
No. 4	26.6	55.0 − 1.7	16.7	25.0	25.1	62.6	1.1	1.18
No. 5	30.8	65.0 + 1.0	18.0	27.3	31.0	78.4	1.0	1.58
No. 6	33.9	75.0 − 4.3	19.4	31.5	35.5	83.0	1.0	1.91
No. 7	41.0	85.0 − 2.3	22.8	38.7	43.4	97.3	0.8	2.79
No. 8	45.8	95.0 − 2.4	25.1	43.2	49.3	110.1	0.7	3.48
Re_λ = 147								
No. 1	10.6	25.0 + 2.1	5.9	9.1	11.6	30.1	2.0	0.29
No. 2	13.0	35.0 + 1.0	6.8	11.3	15.3	40.7	2.2	0.44
No. 3	17.1	45.0 + 0.0	8.9	15.1	20.2	54.1	1.6	0.75
No. 4	21.4	55.0 + 0.1	11.0	19.5	25.2	65.5	1.3	1.18
No. 5	23.0	65.0 − 1.2	11.3	19.5	29.3	79.2	1.0	1.36
No. 6	30.0	75.0 − 2.2	15.5	27.2	35.3	84.6	1.0	2.32
No. 7	38.7	85.0 + 1.6	20.5	35.9	44.5	103.0	0.8	3.86
No. 8	48.3	95.0 − 0.7	28.0	49.2	51.5	110.2	0.7	6.02
Re_λ = 235								
No. 1	18.9	25.0 + 7.6	14.9	18.2	14.8	36.0	1.9	0.89
No. 2	23.8	35.0 − 0.4	18.4	21.9	17.1	37.2	1.9	1.42
No. 3	34.7	45.0 + 4.1	28.0	33.5	25.7	52.4	1.4	3.02
No. 4	36.2	55.0 − 0.2	28.0	39.8	27.0	60.2	1.2	3.28
No. 5	40.4	65.0 − 0.2	29.5	47.8	32.3	74.6	1.0	4.09
No. 6	47.0	75.0 − 4.1	32.4	46.7	41.2	90.3	0.9	5.53
No. 7	45.7	85.0 + 1.6	30.2	46.7	42.7	93.6	0.8	5.23
No. 8	53.0	95.0 + 1.0	31.2	56.0	55.3	112.1	0.7	7.04

REFERENCES

Abramson, I. S., "On bandwidth variation in kernel estimates–A square root law," Ann. Stat. **10**(4), 1217–1223 (1982).

Baker, L., Frankel, A., Mani, A., and Coletti, F., "Coherent clusters of inertial particles in homogeneous turbulence," J. Fluid Mech. **833**, 364–398 (2017).

Bayvel, L. and Orzechowski, Z., *Liquid Atomization*, 1st ed. (Taylor Francis Ltd., 1993).

Bec, J., "Multifractal concentrations of inertial particles in smooth random flows," J. Fluid Mech. **528**, 255 (2005).

Boffetta, G., DeLillo, F., and Gamba, A., "Large scale inhomogeneity of inertial particles in turbulent flows," Phys. Fluids **16**, L20–L24 (2004).

Bordas, R., Hagemeier, T., Wunderlich, B., and Thevenin, D., "Droplet collisions and interaction with the turbulent flow within a two-phase wind tunnel," Phys. Fluids **23**(8), 085105 (2011).

Bragg, A. D., Ireland, P. J., and Collins, L. R., "On the relationship between the non-local clustering mechanism and preferential concentration," J. Fluid Mech. **780**, 327–343 (2015).

Charalampous, G. and Hardalupas, Y., "Clustering of mono-disperse and poly-disperse particles in a 'box of turbulence,'" in 7th ICMF 2010, Tampa, FL, USA, 2010.

Chen, L., Goto, S., and Vassilicos, J. C., "Turbulent clustering of stagnation points and inertial particles," J. Fluid Mech. **553**, 143–154 (2006).

Comaniciu, D. and Meer, P., "Mean shift: A robust approach toward feature space analysis," IEEE Trans. Pattern Anal. Mach. Learn. **24**, 603–619 (2002).

Comaniciu, D. and Ramesh, V., "Real-time tracking of non-rigid objects using mean shift," in *Proceedings of Computer Vision and Pattern Recognition IEEE Conference* (IEEE, 2000), Vol. 2, pp. 142–149.

Comaniciu, D., Ramesh, V., and Meer, P., "The variable bandwidth mean shift and data-driven scale selection," in *Proceedings Eighth IEEE International Conference on Computer Vision* (IEEE, Vancouver, BC, 2001), Vol. 1, pp. 438–445.

Crowe, C. T., Schwarzkopf, J. D., Sommerfeld, M., and Tsuji, Y., *Multiphase Flows with Droplets and Particles* (CRC Press, 1998).

Eaton, J. K. and Fessler, J. R., "Preferential concentration of particles by turbulence," Int. J. Multiphase Flow **20**, 169–209 (1994).

George, W. K., *Lectures in Turbulence for the 21st Century* (Chalmers University of Technology, 2006).

Goepfert, C., Marié, J. L., Chareyron, D., and Lance, M., "Characterization of a system generating a homogeneous isotropic turbulence field by free synthetic jets," Exp. Fluids **48**, 809–822 (2009).

Goto, S. and Vassilicos, J. C., "Self-similar clustering of inertial particles and zero acceleration points in fully developed two-dimensional turbulence," Phys. Fluids **18**, 115103 (2006).

Goto, S. and Vassilicos, J. C., "Sweep-stick mechanism of heavy particle clustering in fluid turbulence," Phys. Rev. Lett. **100**, 054503 (2008).

Hardalupas, Y., Taylor, A. M. K. P., and Whitelaw, J. H., "Velocity and size characteristics of swirling liquid-fuelled flames," Proc. R. Soc. A **428**, 129–155 (1990).

Hardalupas, Y., Taylor, A. M. K. P., and Whitelaw, J. H., "Particle dispersion in a vertical round sudden expansion flow," Philos. Trans. R. Soc., A **341**, 411–442 (1992).

Huck, P. D., Bateson, C., Volk, R., Cartellier, A., Bourgoin, M., and Aliseda, A., "The role of collective effects on settling velocity enhancement for inertial particles in turbulence," J. Fluid Mech. **846**, 1059–1075 (2018).

Hwang, W. and Eaton, J. K., "Creating homogeneous and isotropic turbulence without a mean flow," Exp. Fluids **36**, 444–454 (2004).

Jong, J., Cao, L., Woodward, S., Salazar, J., Collins, L., and Meng, H., "Dissipation rate estimation from PIV in zero-mean isotropic turbulence," Exp. Fluids **46**, 499–515 (2008).

Kolmogorov, A. N., "The local structure of turbulence in an incompressible viscous fluid for very large Reynolds numbers," Proc.: Math. Phys. **434**, 1890 (1941).

Lian, H., "Droplet dispersion in homogeneous and isotropic turbulence," Ph.D. thesis, Imperial College London, 2014.

Lian, H., Charalampous, G., and Hardalupas, Y., "Preferential concentration of poly-dispersed droplets in stationary isotropic turbulence," Exp. Fluids **54**, 1525 (2013).

Lian, H., Soulopoulos, N., and Hardalupas, Y., "Evaluation of the topological characteristics of the turbulent flow in a 'box of turbulence' through 2D time-resolved particle image velocimetry," Exp. Fluids **58**, 118 (2017).

Maxey, M. R., "The gravitational settling of aerosol particles in homogeneous turbulence and random flow field," J. Fluid Mech. **174**, 441–465 (1987).

Monchaux, R., Bourgoin, M., and Cartellier, A., "Preferential concentration of heavy particles: A Voronoï analysis," Phys. Fluids **22**, 103304 (2010).

Monin, A. and Yaglom, A., *Statistical Fluid Mechanics* (MIT Press, Cambridge, Mass, USA, 1971).

Obligado, M., Missaoui, M., Monchaux, R., Cartellier, A., and Bourgoin, M., "Reynolds number influence on preferential concentration of heavy particles in turbulent flow," J. Phys.: Conf. Ser. **318**, 052015 (2011).

Pope, S. B., Turbulent Flows (Cambridge University Press, 2000).

Salazar, J. P. L. C., De Jong, J., Cao, L., Woodward, S. H., Meng, H., and Collins, L. R., "Experimental and numerical investigation of inertial particle clustering in isotropic turbulence," J. Fluid Mech. **600**, 245–256 (2008).

Saw, E., Shaw, R., Ayyalasomayajula, S., Chuang, P., and Gylfason, A., "Inertial clustering of particles in high-Reynolds-number turbulence," Phys. Rev. Lett. **100**, 214501 (2008).

Squires, K. D. and Eaton, J. K., "Preferential concentration of particles by turbulence," Phys. Fluids **3**, 1169 (1991).

Sumbekova, S., Cartellier, A., Aliseda, A., and Bourgoin, M., "Preferential concentration of inertial sub-Kolmogorov particles: The roles of mass loading of particles, Stokes numbers, and Reynolds numbers," Phys. Rev. Fluids **2**, 024302 (2017).

Sundaram, S. and Collins, L. R., "Collision statistics in an isotropic particle-laden turbulent suspension. Part 1. Direct numeric simulation," J. Fluid Mech. **335**, 75–109 (1997).

Tagawa, Y., Mercado, M., Prakash, N., Calzavarini, E., Sun, C., and Lohse, D., "Three-dimensional Lagrangian Voronoï analysis for clustering of particles and bubbles in turbulence," J. Fluid Mech. **693**, 201–215 (2012).

Wang, L. P. and Maxey, M. R., "Settling velocity and concentration distribution of heavy particles in homogeneous isotropic turbulence," J. Fluid Mech. **256**, 27–68 (1993).

Warhaft, Z., "Laboratory studies of droplets in turbulence: Towards understanding the formation of clouds," Fluid Dyn. Res. **41**(1), 011201 (2009).

Wood, A., Hwang, W., and Eaton, J. K., "Preferential concentration of particles in homogeneous and isotropic turbulence," Int. J. Multiphase Flow **31**, 1220–1312 (2005).